

## **Defect Engineering for Creating and Enhancing Bulk Photovoltaic Effect in Centrosymmetric Materials**

*Haoxin Mai, Teng Lu\*, Qingbo Sun, Julien Langley, Nicholas Cox, Felipe Kremer, The Duong, Kylie Catchpole, Hua Chen, Zhiguo Yi, Terry J. Frankcombe\* and Yun Liu\**

*Dr. H. Mai, Dr. T. Lu, Dr. Q. Sun, J. Langley, Dr. N. Cox, Prof. Y. Liu, Research School of Chemistry, The Australian National University, Canberra, ACT 2601, Australia*

*E-mail: [teng.lu@anu.edu.au](mailto:teng.lu@anu.edu.au); [yun.liu@anu.edu.au](mailto:yun.liu@anu.edu.au)*

*Dr. T. J. Frankcombe, School of Science, The University of New South Wales, Canberra, ACT 2601, Australia*

*E-mail: [t.frankcombe@adfa.edu.au](mailto:t.frankcombe@adfa.edu.au)*

*Dr. T. Duong, Prof. K. Catchpole, School of Engineering, The Australian National University, Canberra, ACT 2601, Australia*

*Dr. F. Kremer, Dr. H. Chen, Centre for Advanced Microscopy, The Australian National University, Canberra, ACT 2601, Australia*

*Prof Z. Yi, State Key Laboratory of High Performance Ceramics and Superfine Microstructure, Shanghai Institute of Ceramics, Chinese Academy of Sciences, Shanghai, 200050 China*

### Supplementary Note 1. Crystal structure, morphologies of BNO-O<sub>2</sub> and BNO-N<sub>2</sub> thin films

Figures 1 and S1 summarize the structural characterization of the as-prepared BNO thin films. According to X-ray diffraction (XRD) patterns, the Y<sub>2</sub>O<sub>3</sub> and LaNiO<sub>3</sub> (LNO) layers exhibit strong out-of-plane preferential orientations along the [111]\* and [110]\* directions, respectively, while the intense single peak around 28.3° can be indexed as the (121) peak of the orthorhombic BNO (Figure 1a), implying that these polycrystalline BNO films show out-of-plane preferential orientation along the [121]\* direction. All three layers are phase-pure and highly crystalline, and no minor phases are identified regardless of the annealing atmosphere. No remarkable shifts of the major peaks of the BNO thin films was observed when annealed under different atmospheres, indicating that the annealing atmosphere has little effect on the crystal structure of BNO thin films. As a consequence, the orthorhombic BNO structure was used for indexing the electron diffraction patterns in this report. Figure 1b shows cross-sectional TEM images of the BNO thin film annealed under O<sub>2</sub> for 60 minutes (BNO-O<sub>2</sub>) (Figure 1b, top) and under N<sub>2</sub> for 60 minutes (BNO-N<sub>2</sub>) (Figure 1b, bottom). Both of these images indicate that the interface between BNO/LNO and LNO/Y<sub>2</sub>O<sub>3</sub> are sharp and well-defined, and that the thickness of Y<sub>2</sub>O<sub>3</sub>, LNO and BNO layers are 30 nm, 10 nm, and 185 nm respectively. The AFM results indicate that both the BNO-O<sub>2</sub> and BNO-N<sub>2</sub> thin films are composed of small particles (~40 nm) which are aggregated as large grains with size of a few hundred nanometers (Figure S1). Both films exhibit a smooth surface with root square roughness of ~3.5 nm (BNO-O<sub>2</sub>) and ~4.1 nm (BNO-N<sub>2</sub>), respectively. To further understand the structure of the BNO films, cross-sectional HRTEM images of the BNO-O<sub>2</sub> and BNO-N<sub>2</sub> samples were collected and are shown in Figures 1c and 1d, respectively. The clear lattice fringes showing in the images again indicate that both samples are highly crystalline, and the  $d_{121}$  of the BNO layers (3.15 nm) as well as the SAED patterns further confirm the [121]\* preferential orientation of the BNO layers along the out-of-plane direction on the LNO/Y<sub>2</sub>O<sub>3</sub> structure.

### Supplementary Note 2. Defects in BNO-O<sub>2</sub> and BNO-N<sub>2</sub> thin films

Figure S4 shows the Raman spectra of BNO films. For the orthorhombic BNO samples, the major Raman bands at 625 cm<sup>-1</sup> can be attributed to symmetric stretching vibration (A<sub>1g</sub>) of the NbO<sub>6</sub> octahedra (Figure S4b), while the bands at 195 cm<sup>-1</sup> can be assigned to the bond angle bending,  $\nu_6$  (F<sub>2u</sub>), mode of the NbO<sub>6</sub> octahedra, and the bands at 137 cm<sup>-1</sup> and 153 cm<sup>-1</sup> are also the characteristic of orthorhombic BNO (Figure S4a).<sup>1</sup> No bands of other minor phases or compounds are present. Comparing the Raman spectra between the BNO-N<sub>2</sub> and BNO-O<sub>2</sub> thin films, it is found that for the BNO-N<sub>2</sub> thin film, the Raman active modes at 137 cm<sup>-1</sup>, 153 cm<sup>-1</sup> and 195 cm<sup>-1</sup> shift towards to higher wavenumber. For the A<sub>1g</sub> stretching mode, observed at 625 cm<sup>-1</sup>, despite the main peak position remain unchanged for BNO-N<sub>2</sub> and BNO-O<sub>2</sub> samples, a tiny shoulder appears in the BNO-N<sub>2</sub> sample at higher wavenumber. Furthermore, the Raman bands of BNO-N<sub>2</sub> sample are broader than those of BNO-O<sub>2</sub>. As the morphologies, average structure, and particle sizes of these two thin films are indistinguishable, the broadening and shift of the Raman active modes can be assigned to the presence of defects, *e.g.*, oxygen vacancies in the crystal lattice.<sup>2,3</sup>

X-ray photoelectron spectroscopy (XPS) spectroscopy supports this interpretation of the Raman data. Figures 3a-3d, S5 and S6 show the binding energy of the O 1s, Bi 4f and Nb 3d electrons in the set of BNO thin films annealed under different atmospheres and for different durations. Figures 3a-3d shows the O 1s XPS results for the BNO-O<sub>2</sub> film and the BNO films annealed under N<sub>2</sub> with different annealing time. The O 1s peak at 530.1 eV is attributed to lattice oxygen, while the peak located at 532.5 eV can be assigned to the presence of loosely bound oxygen on the thin film surface, which are normally considered to be surface absorption and contamination.<sup>4</sup> The medium binding energy component centered at about 531.6 eV is associated with oxygen deficient regions within the BNO lattice.<sup>4</sup> Importantly peak intensities in XPS are proportional to the concentration of the oxygen vacancies. To investigate the influence of annealing time on the concentration of the oxygen vacancies, we plotted the  $I_{531}/I_{530}$ , *i.e.*, the ratio of the area of the peak at 531.6 eV ( $I_{531}$ ) to that of the peak at 530.1 eV ( $I_{530}$ ), as a function of the N<sub>2</sub> annealing time. It is worth noting that the  $I_{531}/I_{530}$  ratio of the BNO-O<sub>2</sub> sample is representative of the oxygen vacancies formed initially, rather than those being formed from annealing in an oxygen deficient environment. The  $I_{531}/I_{530}$  values *vs.* N<sub>2</sub> annealing time are plotted in Figure 3e. Note that the  $I_{531}/I_{530}$  ratio of the BNO-O<sub>2</sub> sample is set as  $t=0$  in N<sub>2</sub> annealing time experiment. The linear relationship between the N<sub>2</sub> annealing time and the  $I_{531}/I_{530}$  values indicates that the generation of oxygen vacancies correlates strongly with the N<sub>2</sub> annealing time.

Figure S5 shows the Bi 4f XPS spectra of various BNO samples. For the BNO-O<sub>2</sub> thin film, two typical Bi 4f<sub>7/2</sub> and Bi 4f<sub>5/2</sub> peaks are observed located at 159.4 eV and 164.7 eV, which are typical of Bi<sup>3+</sup>-O bonds.<sup>5</sup> As only a single peak is observed in the Bi 4f<sub>7/2</sub> and Bi 4f<sub>5/2</sub> region, the BNO-O<sub>2</sub> film has a uniform coordination environment for all Bi ions. After annealing in N<sub>2</sub> atmosphere, these peaks split into three (a triplet), with the most intense peak centered at the same binding energy as seen for the BNO-O<sub>2</sub> film. It is attributed to lattice Bi<sup>3+</sup> ions. The other two peaks, indicating new Bi<sup>3+</sup> environments introduced through N<sub>2</sub> annealing, are red-shifted and blue-shifted with respect to the lattice transition. These are assigned to defect regions (Figures S5b – d). A similar peak splitting is also found in the Nb 3d spectra of the BNO-N<sub>2</sub> films (Figure S6). The Nb 3d<sub>3/2</sub> and Nb 3d<sub>5/2</sub> region of the XPS spectrum of the BNO-O<sub>2</sub> film exhibit single peak (206.9 eV and 209.7 eV, respectively), which can be attributed to lattice Nb<sup>5+</sup> ions.<sup>6</sup> In contrast, all the BNO-N<sub>2</sub> samples show small additional blueshifted shoulders on both the Nb 3d<sub>3/2</sub> and Nb 3d<sub>5/2</sub> (207.5 eV and 210.5 eV respectively, Figures S6b-d). The emergence of these new blueshifted shoulders again indicate new Nb<sup>5+</sup> environments introduced through N<sub>2</sub> annealing. Importantly, these results are inconsistent with the formation of a population of Nb<sup>4+</sup>, because Nb<sup>4+</sup> instead has a much lower binding energy.<sup>7</sup> Since peak splitting is found in the Bi 4f band and the Nb 3d band of the BNO-N<sub>2</sub> samples, and the relative intensities of the new peak intensities vary systematically with increasing the annealing time (Table S1), it can be deduced that these new peaks arise from defect structures and that the defect concentration increases on increasing the N<sub>2</sub> annealing time.

The ratios of different peak areas in the XPS spectra were further analyzed to gain a deeper insight of the defect structures (Table S1). As described earlier, the Bi 4f peaks at 159 eV and Nb 3d peaks at 207 eV are assigned to the lattice Bi<sup>3+</sup> and Nb<sup>5+</sup>, respectively,<sup>5, 6</sup> and can be used as an internal reference. It is readily observed that the concentration of defect region (to the lattice) increases with increasing the N<sub>2</sub> annealing time, indicated by

the ascending values of the  $I_{157}/I_{159}$ ,  $I_{160}/I_{159}$  in the Bi 4f band and the  $I_{208}/I_{207}$  in the Nb 3d band. It is intriguing to find that the  $I_{157}/I_{160}$  in the Bi 4f band remains almost constant in all the BNO-N<sub>2</sub> samples. As the Bi 4f peaks at 157 eV and 160 eV are both sensitive to metal ion defects formed under oxygen deficient environment, we propose that these two peaks originate from the same defect regions. In other words, the defect structure formed in the oxygen deficient atmosphere can give rise to two different coordinated environments for the Bi<sup>3+</sup>. Calculations show that the acceptor defect Bi<sub>Nb</sub><sup>''</sup> and the donor defect V<sub>O</sub><sup>••</sup> have the lowest energy of formation in an oxygen poor environment.<sup>8</sup> Considering that no characteristic Nb<sup>4+</sup> peaks are obtained in the XPS results, it is believed that other typical acceptor defects such as Nb<sub>Nb</sub><sup>'</sup> do not exist in these samples. To retain the electrical neutrality of the sample, we suggest that Bi<sub>Nb</sub><sup>''</sup> is generated along with the formation of oxygen vacancies, and the coupled acceptor-donor defects form the defect dipole expressed as Bi<sub>Nb</sub><sup>''</sup> - V<sub>O</sub><sup>••</sup>. Figures 2b and c portray the BNO crystal structure with V<sub>O</sub> and Bi<sub>Nb</sub><sup>''</sup>. When a Nb<sup>5+</sup> ion is substituted by a Bi<sup>3+</sup> (labelled as Bi1), the coordination environments of two neighboring Bi<sup>3+</sup> (labelled as Bi2) are directly influenced by the oxygen vacancy. Moreover, when comparing the total areas underlying the Bi 4f and Nb 3d peaks in different samples, it is found the BNO-N<sub>2</sub> sample has larger Bi/Nb ratio than that of the BNO-O<sub>2</sub> sample, which is consistent with the proposed Bi<sub>Nb</sub><sup>''</sup> defect.

**Table S1.** The ratios of the XPS peak areas in O 1s, Bi 4f and Nb 3d bands of different BNO thin films

	BNO-O <sub>2</sub>	BNO-N <sub>2</sub> 5 min	BNO-N <sub>2</sub> 30 min	BNO-N <sub>2</sub> 60 min
I <sub>531</sub> /I <sub>530</sub> (O 1s)	0.092	0.115	0.179	0.258
I <sub>157</sub> /I <sub>159</sub> (Bi 4f)	-	0.021	0.028	0.031
I <sub>160</sub> /I <sub>159</sub> (Bi 4f)	-	0.090	0.121	0.133
I <sub>157</sub> /I <sub>160</sub> (Bi 4f)	-	0.235	0.231	0.233
I <sub>208</sub> /I <sub>207</sub> (Nb 3d)	-	0.121	0.131	0.141

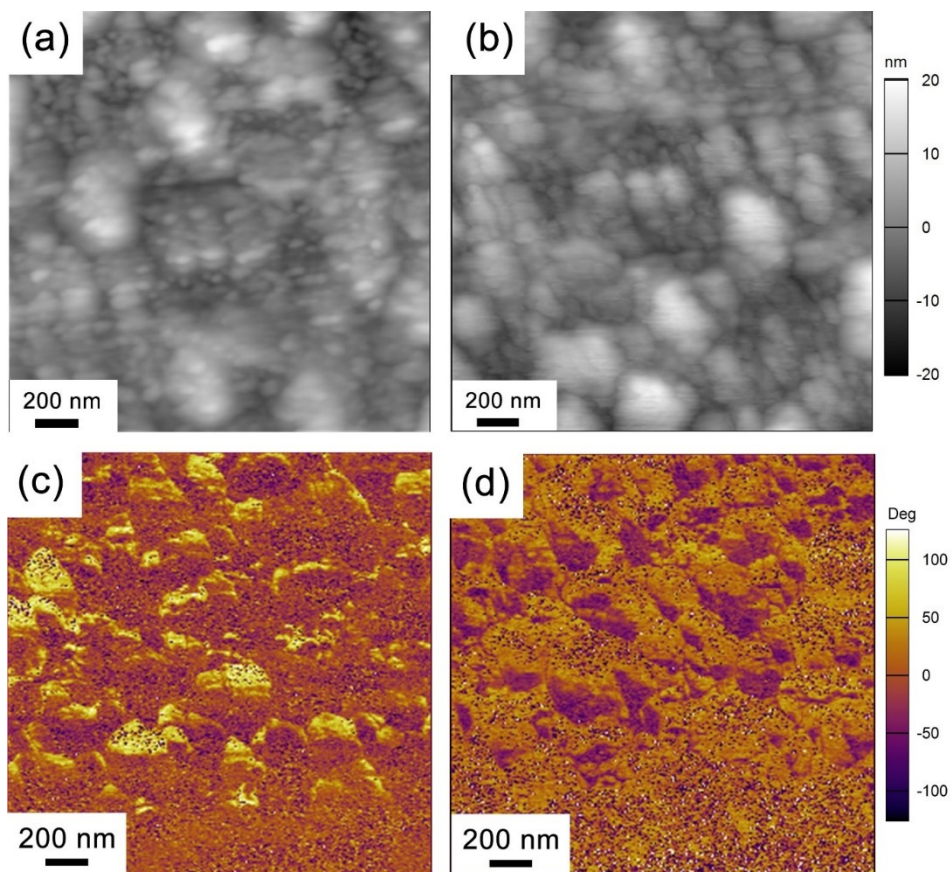


**Figure S1.** AFM images of (a) BNO-O<sub>2</sub> and (b) BNO-N<sub>2</sub> thin films in a 2  $\mu\text{m}$   $\times$  2  $\mu\text{m}$  region. Pristine-state PFM phase images of (c) BNO-O<sub>2</sub> and (d) BNO-N<sub>2</sub> thin films in a 2  $\mu\text{m}$   $\times$  2  $\mu\text{m}$  region.

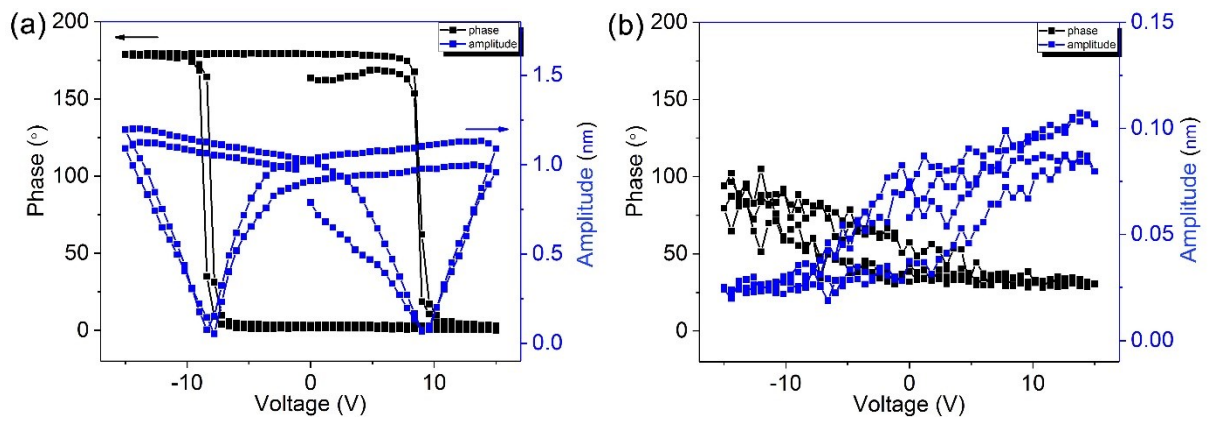


**Figure S2.** The PFM phase-voltage hysteresis loops and amplitude-voltage loops of the (a) BNO-N<sub>2</sub> and (b) BNO-O<sub>2</sub> thin films.

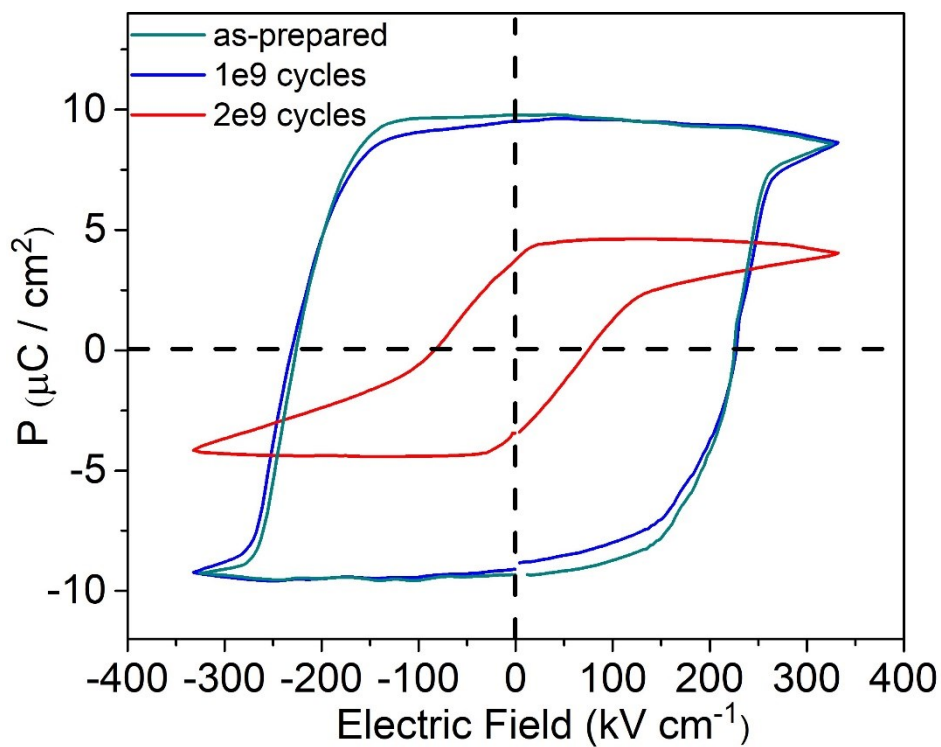


**Figure S3.** Polarization hysteresis in the BNO-N<sub>2</sub> films after different switching cycles.

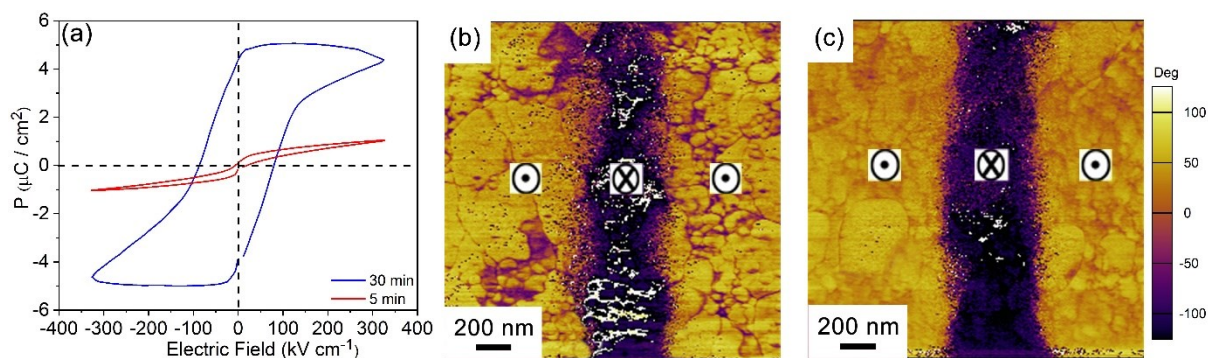


**Figure S4.** (a) Polarization hysteresis in the  $N_2$ -annealed BNO films with different annealing time; the measurement was performed at the frequency of 20 kHz. Domain patterns from a  $2 \mu\text{m} \times 2 \mu\text{m}$  region of the BNO films annealed at  $N_2$  for (b) 5 minutes and (c) 30 minutes; the tip bias applied on the samples are  $\pm 15$  V.

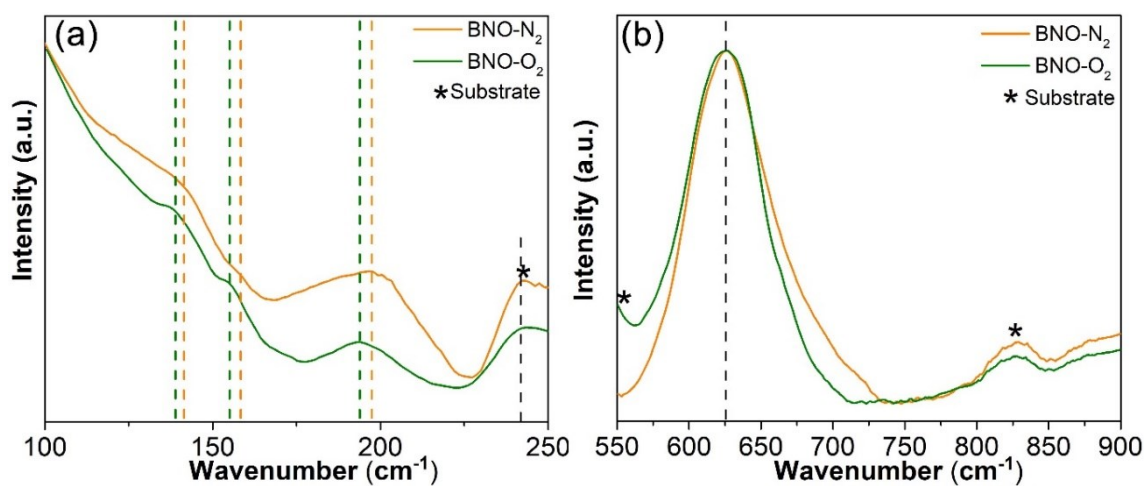


**Figure S5** Raman spectra in the (a)  $100 - 250 \text{ cm}^{-1}$  and (b)  $550 - 900 \text{ cm}^{-1}$  regions for BNO- $N_2$  and BNO- $O_2$  thin films.

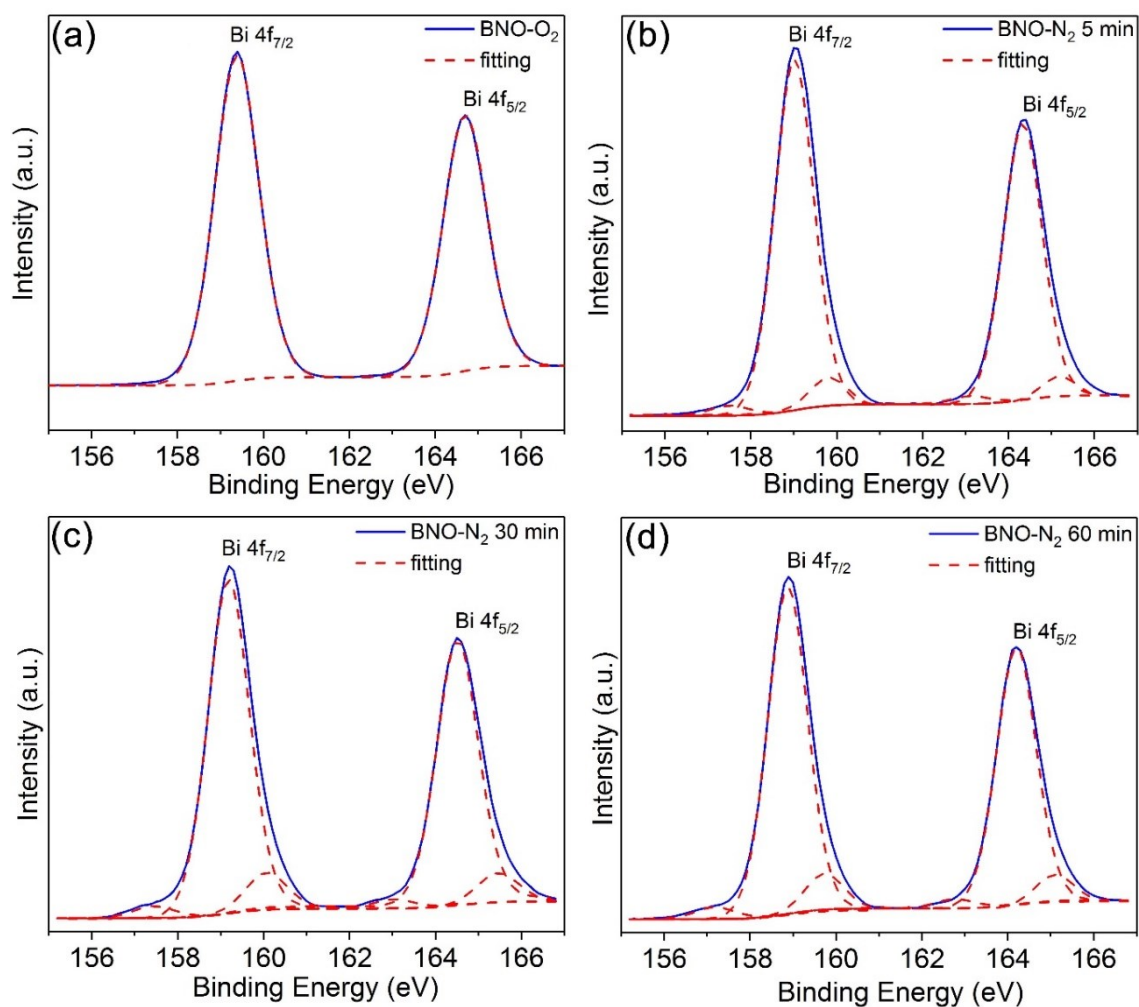


**Figure S6.** XPS spectra of the Bi 4f for (a) a BNO-O<sub>2</sub> film and for BNO films annealed under N<sub>2</sub> for (b) 5 minutes, (c) 30 minutes and (d) 60 minutes. Dash lines represent the fitting curves to Gaussian distribution.

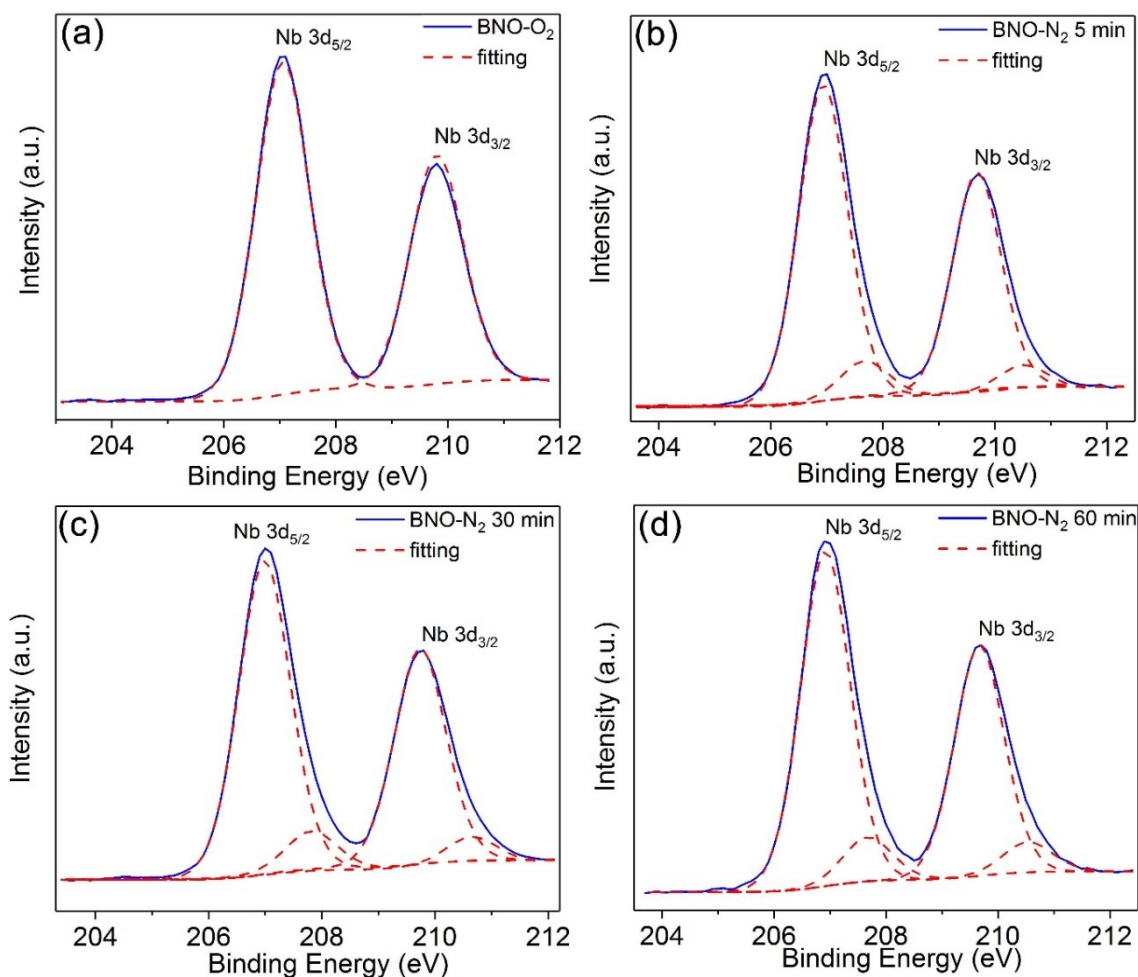


**Figure S7.** XPS spectra of the Nb 3d for (a) a BNO-O<sub>2</sub> film and for BNO films annealed under N<sub>2</sub> for (b) 5 minutes, (c) 30 minutes and (d) 60 minutes. Dash lines represent the fitting curves to Gaussian distribution.

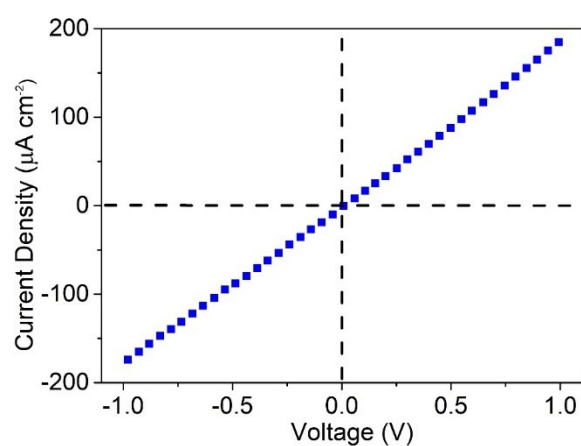


**Figure S8.** Current-voltage curve for a BNO-O<sub>2</sub> thin film under AM 1.5 G (100 mW cm<sup>-2</sup>) illumination. The top electrode is ITO, and the bottom electrode is LNO. Both the open circuit voltage and the short circuit

current density is  $\sim 0$ . As the work functions of ITO (4.5 eV) and LNO (4.4 eV) are almost identical, the built-in field is negligible. Therefore, no PV effect can be observed in this sample.

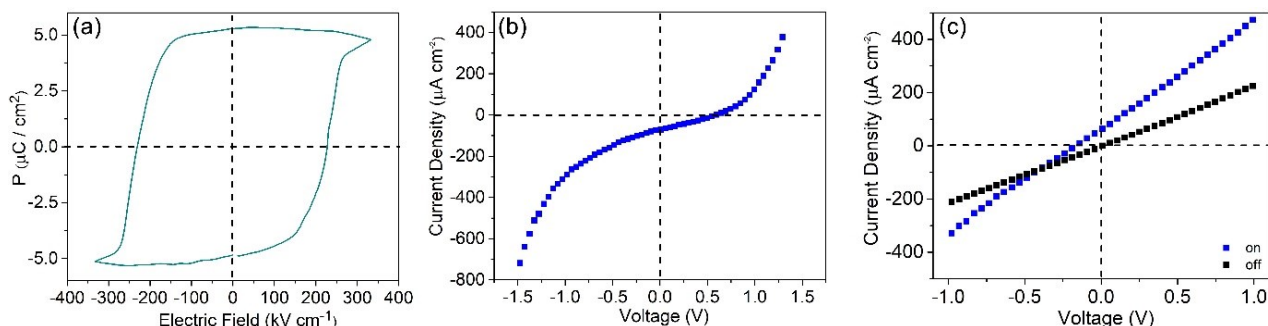


**Figure S9.** (a) Polarization-voltage hysteresis loop for the BNO-N<sub>2</sub>/BNO-O<sub>2</sub> structure. Current-voltage curve for the (b) positive poled and (c) non-poled BNO-N<sub>2</sub>/BNO-O<sub>2</sub> structure under AM 1.5 G (100 mW cm<sup>-2</sup>) illumination. The poling voltage is 10 V, and the poling time is 10 minutes.

## Reference

1. P. Ayyub, M. S. Multani, V. R. Palkar and R. Vijayaraghavan, *Phys. Rev. B*, 1986, **34**, 8137-8140.
2. M. M. Khan, S. A. Ansari, D. Pradhan, M. O. Ansari, D. H. Han, J. Lee and M. H. Cho, *J. Mater. Chem. A*, 2014, **2**, 637-644.
3. S. H. Chen, Y. Xiao, Y. H. Wang, Z. F. Hu, H. Zhao and W. Xie, *Nanomaterials-Basel*, 2018, **8**.
4. J. P. Wang, Z. Y. Wang, B. B. Huang, Y. D. Ma, Y. Y. Liu, X. Y. Qin, X. Y. Zhang and Y. Dai, *ACS Appl. Mater. Inter.*, 2012, **4**, 4024-4030.
5. Y. L. Zhang, Y. H. Wang, J. Qi, Y. Tian, M. J. Sun, J. K. Zhang, T. J. Hu, M. B. Wei, Y. Q. Liu and J. H. Yang, *Nanomaterials-Basel*, 2018, **8**.
6. C. Zhou, Y. F. Zhao, L. Shang, Y. H. Cao, L. Z. Wu, C. H. Tung and T. R. Zhang, *Chem. Commun.*, 2014, **50**, 9554-9556.
7. T. Joshi, P. Borisov and D. Lederman, *J. Appl. Phys.*, 2018, **124**, 114502.
8. K. R. Lai, Y. T. Zhu, Y. Dai and B. B. Huang, *J. Appl. Phys.*, 2012, **112**.